

# Study on Drag Coefficient ( $C_D$ ) Value of Low-Energy Prototype Class Car

J. Jodiputra, S. Tobing\*, H. Gunawan,  
Mechanical Engineering Department  
Faculty of Engineering, Atma Jaya Catholic University of Indonesia  
Banten, Indonesia  
[\\*sheila.tobing@atmajaya.ac.id](mailto:*sheila.tobing@atmajaya.ac.id)

M.G. Andika  
National Laboratory for Aerodynamics, Aeroelastics, and Aero-Acoustics  
Technology, The Agency for Assessment and Implementation of Technology  
(BPPT), Banten, Indonesia

## ABSTRACT

Researches on car design are closely related to the field of aerodynamics. The design was done to minimize the drag force. The experimental method was only used for testing the initial design and the final design. Improvement and modification were done by using the CFD simulation. The experiments were done using the Low Speed Wind Tunnel (LSWT) owned by the National Laboratory for Aerodynamics, Aeroelastics, and Aeroacoustics Technology. The Reynolds number ranged from 505,225 to 671,528. The research began with the initial design called JM-5, tested in the LSWT. Modifications were done throughout the research to achieve the lowest drag coefficient value. In the end, JM-4v2 became the final design with the lowest drag coefficient value of 0.202.

**Keywords:** Low-energy prototype class car, Coefficient of drag, Low Speed Wind Tunnel, CFD; KMHE car

## Nomenclature

$C_D$	Drag coefficient value
CFD	Computer Fluid Dynamic
JM-5	Model of JM-5
JM-4	Model of JM-4

LSWT	Low Speed Wind Tunnel
Re	Reynolds number
S	Sectional frontal area
V	Velocity

## Introduction

Kontes Mobil Hemat Energi (KMHE) is a competition organized by Direktorat Jenderal Pendidikan Tinggi (DIKTI) on a national scale and followed by many universities in Indonesia. This competition aims to support the creativity of many students from various institutions or universities in creating a low-energy car. The low-energy car in KMHE divided into two classes, namely urban class and prototype class. Prototype class cars are required to have a design that can minimize energy consumption so that it can go as far as possible [1]. Factors affecting energy consumption in energy-efficient cars are shown in Figure 1. This study focused on examining the effect of aerodynamics on the energy consumption of a low-energy prototype class car [2].

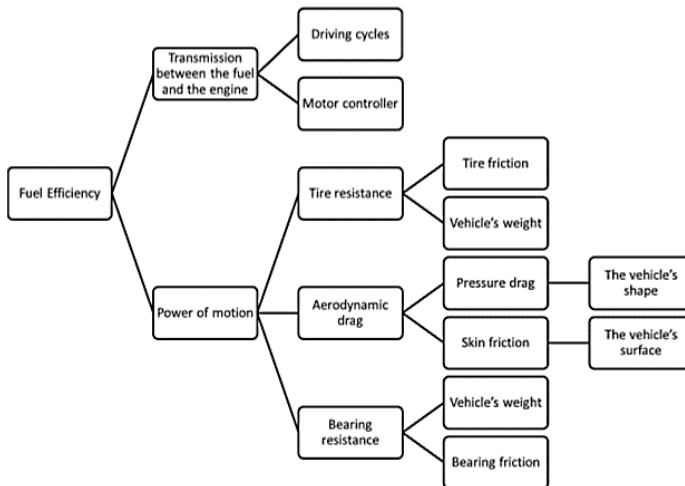


Figure 1: Factors affecting the energy consumption of low-energy car [2]

Aerodynamic studies of drag coefficients were done by Eugene from Mapua Institute of Technology Philippines. Team Cardinals 2012 successfully created a low-energy prototype class car, named Aguila. Aguila's body was built with a length of 2.59 m and a frontal area of 0.32 m<sup>2</sup> (without wheels).

Through simulation done on CATIA V5 software, Aguila showed a drag coefficient value of 0.3 within a constant velocity of 16.67 m/s (equal to 60 km/h). The simulation was conducted only on the car body without considering the effects of the wheels. The team participated in the Shell Eco-marathon Asia race in 2012 [3].

Aerodynamic studies were also conducted by Danek, a student of the Silesian University of Technology in Poland. Danek conducted an aerodynamic study on a low-energy prototype class car called MuSHELLka. MuSHELLka had a length dimension of 2.75 m with a frontal area of 0.297 m<sup>2</sup> (including wheels). The open-wheel configuration was applied to the front wheels which were located outside the body. Through simulation done in software ANSYS CFX, MuSHELLka showed a drag coefficient value of 0.255 within a constant velocity of 9.72 m/s (equal to 35 km/h). Unlike the previous literature, MuSHELLka simulation was done with the wheel-mounted, like the real one. MuSHELLka raced in the Shell Eco-marathon competition in 2012 and finished in the 10<sup>th</sup> position [4].

Things were slightly different from the simulation conducted by Abo-Serie from Konya Mevlana University in Turkey. They simulated the low-energy prototype class car called Eco-Rumi with a wheel enclosed by a disc-shaped cover separated from the body. Eco-Rumi had a length dimension of 2.9 m with a frontal area of 0.265 m<sup>2</sup> (with a covered wheel). The simulation of aerodynamics was done by using STAR CCM+ software and showed a drag coefficient value of 0.127 within a constant velocity of 7.3 m/s (equal to 26,28 km/h) [5].

Like MuSHELLka, Cieslinski from the Lodz University of Technology conducted an aerodynamic study on different cars, Eco Arrow Prototype 3. Eco Arrow Prototype 3 had the same open wheel configuration as MuSHELLka. Eco Arrow Prototype 3 had a length of 3.1 m with a frontal area of 0.25 m<sup>2</sup> (with open wheels). When fairing was used as a wheel cover, the frontal area became 0.27 m<sup>2</sup>. Eco Arrow Prototype 3 car simulation was done by using ANSYS FLUENT software with two different conditions: with the fairing and without the fairing. As a result, the car with fairing showed a lower drag coefficient value of 0.182, while the other one without fairing showed a drag coefficient value of 0.197 [6].

Similar to Aguila, a CFD simulation conducted by Joshua also focused on the car's body. He used Antawirya Turangga Veda as the initial model (built by the Antawirya team, University of Diponegoro) and Antawirya Turangga Veda II as the final model. Changes were made on the front and rear sections of the car. He modified the front and rear sections of the car with narrower design. The simulation ran on four velocities variables and the Reynold numbers ranged from About 19% decrement of  $C_D$  value was obtained from 0.262 to 0.213 [7].

## **Methodology and setup**

This study used two types of testing methods: experimental testing and CFD. Experimental testing was conducted by using Low Speed Wind Tunnel (LSWT) owned by National Laboratory for Aerodynamics, Aeroelastics, and Aeroacoustics. An experimental test was only performed on the initial and final model, while CFD was done in between. CFD was conducted for the development and improvisation of the model design to produce the lowest drag coefficient value. All models used in the experimental testing were made by using 3D printers with PLA filament printing material. For CFD, the models were made by using SOLIDWORKS 2015 and the analysis was done by using ANSYS Fluent 17.2. The whole development and improvisation design were also done by using SOLIDWORKS and ANSYS Fluent. This step was carried out to reduce the cost and effort of the research.

### **Methodology and Model**

In this research, the drag coefficient equation was the basic equation. The drag coefficient was a dimensionless value. To be dimensionless, the drag force must be divided against the dynamic pressure multiplied by the frontal area of the model. Equation (1) describes the definition of a drag coefficient. The drag force ( $F_{\text{drag}}$ ) was obtained from the normal pressure ( $p$ ) and the shear stress ( $\tau$ ) along the surface of the model. Then the dynamic pressure was generated by the relative speed of the airflow against the model and had a constant magnitude along with the model [8].

$$C_D = \frac{F_{\text{drag}}}{\frac{1}{2} \rho V^2 A} \quad (1)$$

“ $\rho$ ” was the density ( $\text{kg/m}^3$ ) and “ $V$ ” was the fluid flow velocity ( $\text{m/s}$ ). The unit of the dynamic pressure was Newton per millimeter squared ( $\text{N/mm}^2$ ), which is the unit of pressure. “ $A$ ” value was the frontal area of the model's front view. The frontal area was determined from a certain distance measured from the front end of the car body. The area was a front view of the model seen perpendicularly to the direction of the incoming fluid flow. Thus, the frontal area was measured in two dimensions [9].

As mentioned earlier, there were two models: the initial and the final model. The initial model called JM-5 and the final model called JM-4. Both models were shown at all views in Figure 2, Figure 3, and Figure 4. Then, the steps of development and improvisation from the initial model to the final model were described in the following chart in Figure 5.



(a) (b)  
Figure 3: Rear view of (a) JM-5 as the initial model, and (b) JM-4 as the final model



(a)



(b)

Figure 4: Side view of (a) JM-5 as the initial model, and (b) JM-4 as the final model



Figure 5: The steps of development and improvisation from JM-5 to JM-4 model

In addition to the force measurement (to get the drag coefficient value), wool tuft visualization was also done to get the visualization of air around the model. This wool tuft visualization was compared to the visualization from the CFD. This step was done to validate all CFD results. The installed wool tuft on each model could be seen in Figure 2, Figure 3, and Figure 4. JM-5 model was painted in a different color to make it look different from the JM-4 model.

### Experimental Setup

Low Speed Wind Tunnel was chosen for the experimental testing that used non-aircraft models. The size of the test section was 1.5 m of width and 2 m of length. It supported the 3D printed models with a size of 0.307 m of length, 0.06 meters of width, and 0.048 m of height. The Reynold number ranged from 505,225 to 671,528. In addition, the Reynolds number greater than 500,000 was turbulent flow regimes. Turbulent flow always occurs in reality, thus more and more in line with the events and aerodynamic phenomena in reality.

The scale of the model size was 1:8.1. This scale was set to prevent having a large blockage ratio, which was below 20%. The frontal area of the model (calculated and reviewed on SOLIDWORKS) was 0.00458 m<sup>2</sup>. With the selected model size and test section size at LSWT, the blockage ratio was 1.85%. The blockage ratio was considered low, so it could be ignored. The testing was not interrupted by the size of the test section.

This experimental testing preparation has been done both from modeling to load cell calibration. The position of the model was placed according to Figure 6. Visible model tied with a stem which was then paired using a bolt to the load cell. Because the length of the stem was too short, the load cell position must be elevated to reach the bolt hole in the stem. As a result, the load cell was attached to an acrylic rod and the acrylic rod was clamped by a “C” clamp on the profile beam. In addition to the model, there was also a ground board installed in the test section. Distance from the model to the ground board was as far as 3 mm. This distance was adjusted to make sure that the drag force obtained was not disturbed by the friction between the

model (which was its tire) and the ground board during the test. The ground board was acting as a conveyor replacement, where its function was as the basis of a model and represented the road where the car was moving. However, because the ground board was not moving like a conveyor and the model was made with a fixed wheel that could not rotate, the ground board function was only as a foundation. The ground board position was arranged as seen in Figure 7 (a), while the position of the model has been done with the help of laser alignment as seen in Figure 7 (b).

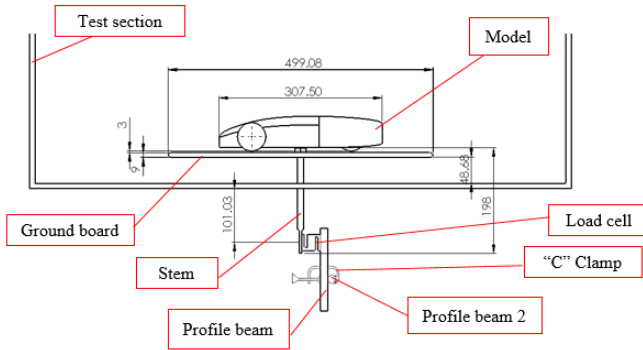


Figure 6: Experimental testing scheme

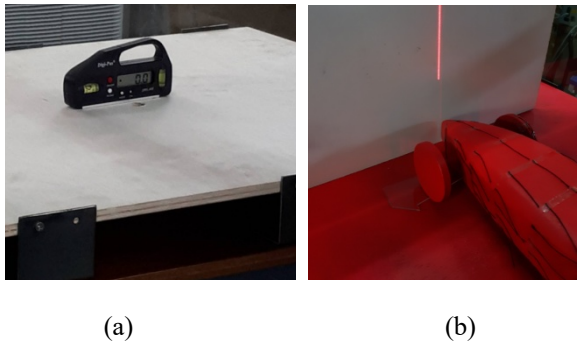


Figure 7: (a) Adjustment of the ground board and (b) alignment of the model by using laser alignment

### CFD Setup

CFD simulation was done using ANSYS 17.2 software. The model geometry was made using SOLIDWORKS 2015 software. The model was placed inside two pieces of domain, the primary domain and a smaller domain named car box. Both domains were air. The model was made on a 1:8.1 scale and all sides of the car were used for computing. Detailed display of domain dimensions and placement are shown in Figure 8.

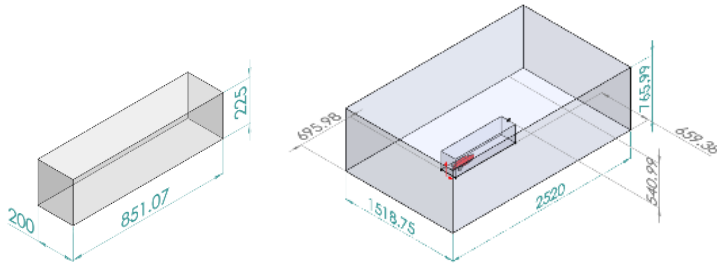


Figure 8: Detail of domain dimensions and placement

The meshing process was done on ANSYS ICEM CFD. Meshing with a tetrahedral form was applied across domains and the model. The total elements generated range from 4 million to 5 million elements. The meshing process is done on sub software ANSYS ICEM CFD. Meshing with a tetrahedral form is uniform across domains and models. The total elements used range from 4 million to 5 million elements. The size of elements used in domains, car boxes, and the model was as in Table 1.

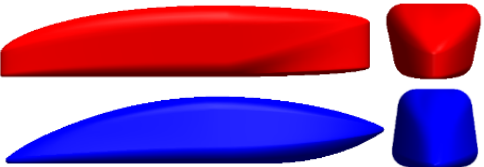
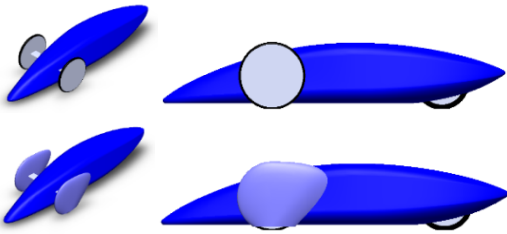
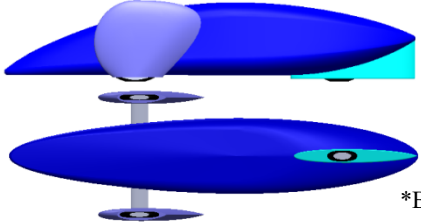
Table 1: Size of element used

Object	Sizing	Size type	Element size
Domain	Global sizing	Element size	Min.: 0.002 m Prox. Min. Size: 0.005 m
Car box	Body sizing	Body of influence	0.005 m
Model	Face sizing	Element size	0.004 m
Model	Inflation	First layer thickness	First layer height: 0.000854 m Max. layers: 10 Growth rate: 1.15

The flow simulation was performed by using Fluent. The simulations were run based on the Navier-Stokes equations under the  $k-\omega$  SST turbulent model at a steady state. The air density was assumed to be constant at  $1.225 \text{ kg/m}^3$ . The Reynolds ranged from 505,225 to 671,528. The dynamic viscosity was constant at  $1.789 \times 10^{-5}$ .

Table 2 listed the geometries tested in the CFD as a modification from the JM-5 model into a JM-4 model.

Table 2: Geometries tested in the CFD

Geometry	Picture
JM-5 (red) & JM-4 (blue)	
JM-4 with unclosed wheel and closed front wheel	
JM-4 with the closed front wheel and closed rear wheel	 <p style="text-align: right;">*Bottom view</p>

## Results and discussion

### Experiment Results for Initial Design

Experimental testing was done by testing in three Reynolds numbers, as shown in Table 3.

Table 3: Result from experimental and CFD testing for JM-5 model

Re	$C_D$ Exp.	$C_D$ CFD	Error
505.225	0,362	0,269	25,69%
557.853	0,375	0,302	19,47%
610.480	0,391	0,341	12,79%

It appears that the higher the Reynolds number, the greater the value of the drag coefficient ( $C_D$ ). It seemed not aligned with Equation (1), where the higher the speed, the value of the  $C_D$  should decrease. It was not wrong if the drag force ( $F$ ) felt by the object (in this case is that the car body) is constant. However, in this experimental data, this upward trend indicates that as the speed increases, the drag force that felt by the car body was also getting more significant. In other words, the increase in the drag force felt by the car body will be proportional to the dynamic pressure multiplied by the frontal area ( $A$ ).

It appeared that the error between experimental results and CFD simulation result is quite large. This was due to various factors. The first factor was friction on the surface of the model that could be contributed to the drag force. In the CFD simulation, the type of material is negligible so there was undoubtedly a difference with experimental results. The second factor was the turbulent model on CFD simulation. Turbulence in the real-life could not be modeled 100% identical in CFD simulations. The CFD simulations are limited to the resources of the computer so that turbulence modeling should be simplified. One way to simplify the turbulence was averaging flow fluctuations as applied in the  $k-\omega$  SST turbulent model as a member of the RANS (Reynolds Averaged Navier Stokes). The third factor was the occurrence of undesirable moments that happened on the stem that holding the model. When performing the test, the load cell used was only 1 unit and it was located outside of the bottom of the test section. In contrast to the airfoil test using 2 load cells mounted on the left side and the right side outside the test section. With only 1 load cell and long stem length (about 450 mm), there was an unexpected and undesirable moment during the test. This moment was seen in the value of the load cell, the force shall show a positive value (compression), but it showed a negative value. After making some precise arrangements, the negative value was overcome but due to only one load cell was used and the length of the stem, this factor could be still the cause of a significant error.

### Wool tuft visualization

Figure 9 shows the wool tuft visualization on the front section of the JM-5 model. In this section, the wool looked not showing any movement. Stating that the steady wool condition was visible from the similarity of wool conditions on the sequence of picture (Figure 9) from left to right. In the absence of vibration and steady wool behavior as well as the direction of this freestream, it could be stated that there had been no point of separation yet and the airflow was still attached and flowing smoothly on the surface of the front section of the JM-5 model. This means that on the front section of the JM-5 model has not seen as the source of the drag force.



Figure 9: Wool tuft visualization on the front section of JM-5 model

In Figure 10, it appears that some of the wool on the middle section of the JM-5 model had started to not be aligned with the freestream direction and some of it was already visible blurred. The wool that not aligned with the freestream indicates the potential for flow to separate, while the blurred wool indicates at that point the airflow had separated from the JM-5 model and resulted in the creation of wakes that could contribute a significant drag force.

Seen in Figure 11, that most of the wool on the rear section of the JM-5 model was blurred. From this blurred look, it could be said that the wool had vibrated and signified the occurrence of airflow separation before reaching the rear end of the JM-5 model. This suggested that the separation point on the back of the JM-5 model occurred too early and would produce large wakes. Wakes occurred in contrast at the rear end of the JM-5 model as shown in Figure 11. It appears that the entire wool is faded and certainly vibrates indicating a large area of wakes occurred behind the JM-5 model.

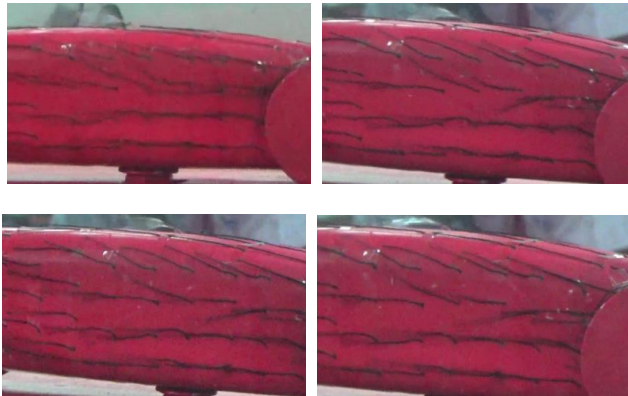


Figure 10: Wool tuft visualization on the middle section of JM-5 model

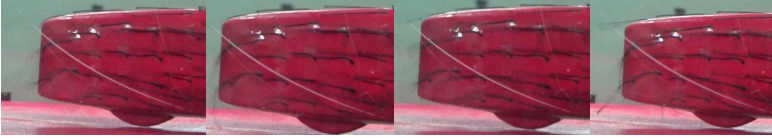


Figure 11: Wool tuft visualization on the rear section of JM-5 model

## CFD Simulation

### Comparing the body of the models

After knowing the  $C_D$  value of the JM-5 model, JM-4 was created as a new model. The JM-4 model had a different length and it affected the Reynold number. In addition to the length, the nose and tail shape of the JM-5 model also changed. The changes were seen in Table 2.

Table 4: Results of JM-5 model and JM-4 model in CFD

Model	Re	$C_D$ CFD	$C_D$
JM-4	555.748	0,0912	0,170
	613.638	0,167	
JM-5	671.529	0,252	0,183
	505.225	0.104	
	557.853	0.177	
	610.480	0.267	

This section of simulation only analyzes the body of the models (without the wheels). Table 4 showed that the  $C_D$  value of the JM-4 model was 7.64% lower than the JM-5 model. This showed that the change in length, the nose shape, and the tail shape on the model JM-5 managed to minimize the drag force. This was consistent with the literature which says that the lower nose shape and smaller tail form could decrease the  $C_D$  value [10]. This statement was supported by the visualization from CFD results in Figure 12 and Figure 13.

Figure 12 showed the visualization of static pressure contour on the front section of the JM-5 model and JM-4 model. The red area was the area of static pressure. The static pressure on the front of the model also called the stagnation point and could inhibit the car's movement as it contributed to the drag force. It was clear that the red area on the front of the JM-5 model was more significant than the JM-4 model. It was stated that the significant pressure on the front of the JM-5 model contributed more drag force so that the  $C_D$  value would increase. Aside from the stagnation point, the cause of the drag force was wakes that occurred behind the model. Wakes occurred because of the

drastic difference in pressure resulting in a gradation of adverse pressure, creating a vacuum effect on the rear section of the car. In Figure 13, wakes were marked with a blue area. It appeared that the wakes on the JM-5 model weremore extensive than the JM-4 model. The wakes area on the JM-5 model was more extensive because the shape of the tail of the JM-5 model was larger than the JM-4 model. With a larger tail, the lower-pressure region at the rear of the model got bigger. The enlargement of the lower pressure region increased the encounter between the higher pressure and the lower pressure so that the wakes region gets bigger. From these two visualizations, it could be stated that the JM-5 model had a more significant drag force than the JM-4 model, so the JM-4 model had resulted in lower  $C_D$  value. Thus, the JM-4 model was chosen to be modified further.

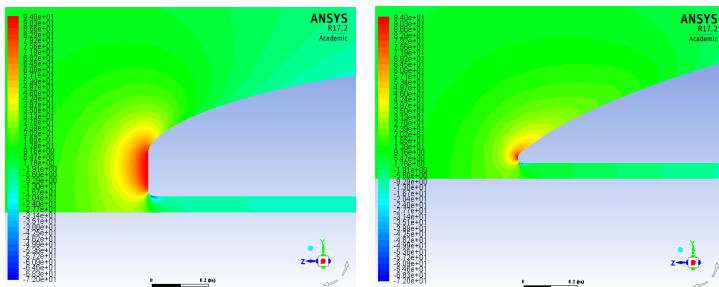


Figure 12: Contour of static pressure on the front section of JM-5 model (left) and JM-4 model (right)

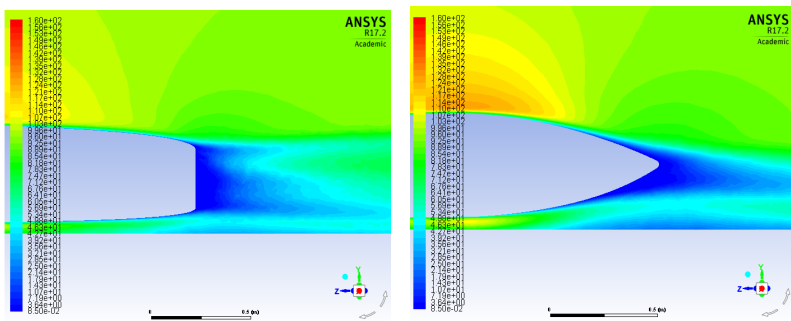


Figure 13: Contour of dynamic pressure on the rear section of JM-5 model (left) and JM-4 model (right)

Front wheel cover

The simulation results in Table 5 showed that the design of the car with the front wheel that had been covered successfully produced a lower  $C_D$  value of 0.243. The covered front wheel successfully decreased the  $C_D$  value by 13.67% before the front wheel was closed. This indicated that the use of a cover on the front wheel had a significant role in reducing the  $C_D$  value.

Table 5: Results of the JM-4 model with the uncovered front wheel and covered front wheel

Front wheel	Re	$C_D$ CFD	$C_D$
Uncovered	555.748	0.165	0.291
	613.638	0.283	
	671.529	0.424	
Covered	555.748	0.155	0.256
	613.638	0.243	
	671.529	0.369	

The contour of dynamic pressure shown in Figures 14 and Figure 15 illustrated the comparison between the uncovered and covered front wheels. It could be seen that in Figure 14 there was a shrinkage of wakes region when the wheel was covered. The shrinkage of the wake area was more visible from the top view, as in Figure 15. The shrinkage of the wake area had successfully reduced the  $C_D$  value by 13.67% from the uncovered wheel. The wakes area was minimized due to the shape of the cross-section of the cover that resembles airfoil (viewed from the top view).

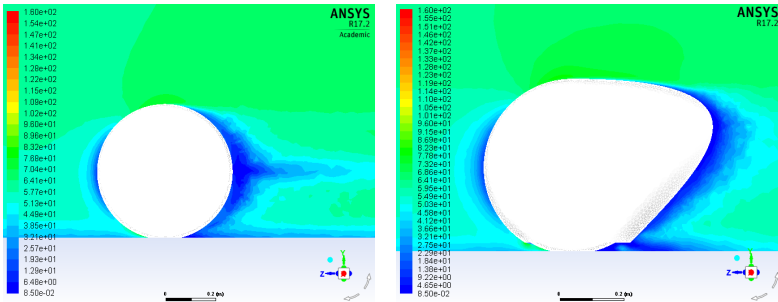


Figure 14: Contour of dynamic pressure on the uncovered front wheel (left) and covered front wheel (right) from the side view

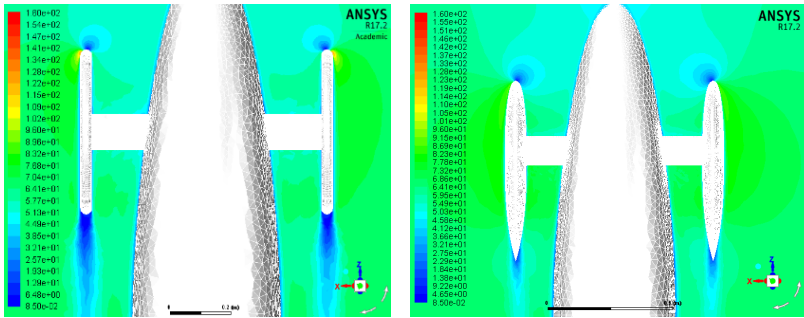


Figure 15: Contour of dynamic pressure on the uncovered front wheel (left) and covered front wheel (right) from the top view

### Rear wheel cover

Table 6 showed the simulation results of the effect of the rear wheel cover on decreasing the  $C_D$  value. It shall be noted that the uncovered rear wheel condition was already covered front wheel and the rear wheels had not been covered. This means that the  $C_D$  value on the uncovered rear wheel was the same as the covered front wheel in the previous section. The simulation results in Table 6 showed that the rear wheel cover successfully decreased 26.73% of the  $C_D$  value in the JM-4 model. This indicated that the use of the rear wheel cover had the same role as the front wheel cover in terms of reducing the  $C_D$  value.

Table 6: Results of the JM-4 model with the uncovered rear wheel and covered rear wheel

Rear wheel	Re	$C_D$ CFD	$C_D$
Uncovered	555.748	0.155	0.256
	613.638	0.243	
	671.529	0.369	
Covered	555.748	0.168	0.202
	613.638	0.201	
	671.529	0.236	

By installing the rear wheel cover, the area of the wake was minimized successfully. It could be seen in Figure 16 that the wakes region was minimized by delaying the encounter between the higher-pressure stream and the lower pressure, which becomes the outset of wakes. Following the results of the previous test, the cross-sectional shape of the rear wheel cover was also made to resemble an airfoil to minimize the drag force. This proved successful because the area of the wake had been narrowed down, shown in Figure 17.

Thus, the rear wheel cover was recommended for installation to minimize the value of the  $C_p$ .

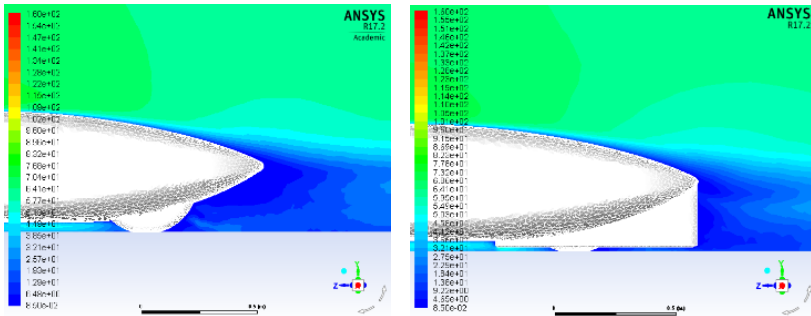


Figure 16: Contour of dynamic pressure on the uncovered rear wheel (left) and covered rear wheel (right) from the side view

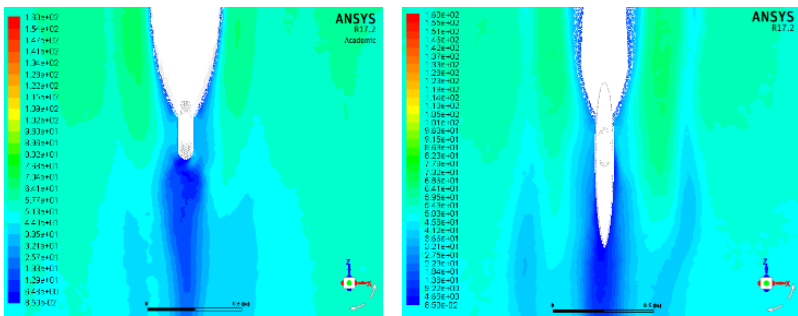


Figure 17: Contour of dynamic pressure on the uncovered rear wheel (left) and covered rear wheel (right) from the side view

### Experiment Results for Final Design

The final design in this research was the JM-4 model that had been installed front wheel cover, and rear wheel cover. So, this final design was named the JM-4 v2 model. Table 7 showed the results of experimental testing on the final design. It appeared that the value of the  $C_D$  was still increasing as the Reynolds number increased. Although the error was quite large, but this upward trend was still in accordance with the CFD simulation had done. The cause of the error had been discussed in the previous sections.

Table 7: Result from experimental and CFD testing for JM-4 model

Re	$C_D$ Exp.	$C_D$ CFD	Error
555.748	0,276	0.168	39.13%
613.638	0,283	0.201	28.98%
671.529	0,290	0.236	18.62%

### Wool tuft visualization

Figure 18 showed the wool tuft visualization on the front section of the JM-4 v2 model. It appeared that the whole wool behavior seen on the front of the JM-4 v2 model was still steady and parallel with the freestream. It was also noticed that there was no vibrated wool caused by airflow. Steady wool behavior and no vibrated wool indicated that there had been no separation point and the airflow still attached to the surface of the front section of the model. Thus, in this section, there was no significant drag force yielded yet.

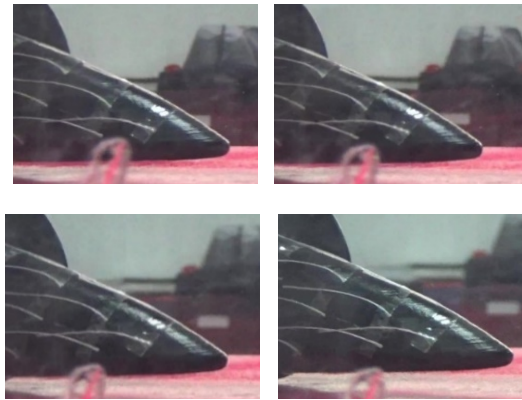


Figure 18: Wool tuft visualization on the front section of the JM-4 v2 model

The difference between the JM-4 v2 model with the JM-5 started from the middle section to the rear section. In Figure 19, it appeared that the wool on the middle section of the JM-4 v2 model was not blurred. This showed that the wool was still steady and showed the airflow still attached to the surface of the body, so it is called the attached flow. In addition, it appeared that the wool was still parallel with the direction of the freestream which indicated that airflow on the middle section of the JM-4 v2 model had not occurred separation and not resulted in a significant drag force.

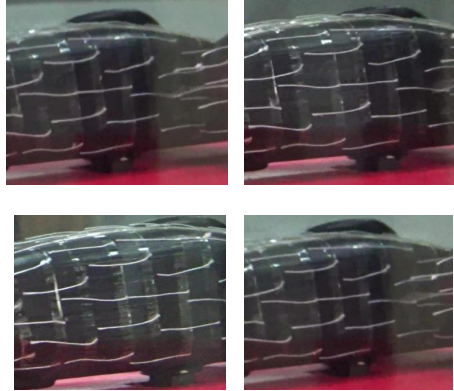


Figure 19: Wool tuft visualization on the middle section of JM-5 model

Figure 20 showed that the wool behavior on the rear section of the JM-4 v2 model was still steady. The wool started to blur at the rear end of the JM-4 v2 model. From this, it could be ascertained that the wool had been vibrated. The wool located at the rear of the model (before the rear end of the model) showed the location of the separation point that became the beginning of the wakes. The area of wakes on this visualization was not fully visible because the area of the wake lay from the rear end of the model until it was completely separated from the model (towards the back). So, wool tuft visualization was only to show the early phases of wakes or when the wool at the end of the model looks blurry or vibrating.

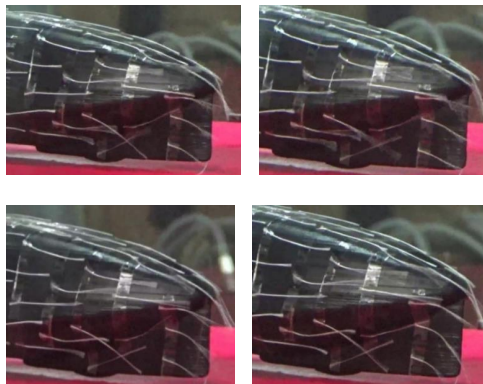


Figure 20: Wool tuft visualization on the rear section of JM-5 model

When comparing the wool tuft visualization between the JM-5 model and the JM-4 v2 model, it was clear that the JM-4 v2 model had better wool tuft behavior than the JM-5 model. This was seen from the middle of both models, where the wool on the JM-5 model had started to vibrate while the JM-4 v2 model did not. Then continue to the rear of the model where the difference was noticeable, that the wool on the JM-5 vibrated more than on the JM-4 v2 model. From the comparison of visualization and CFD result data, it can be stated that the design of JM-4 v2 is the final design with a  $C_D$  value of 0.202.

## **Conclusion**

This study was successfully conducted in both experimental and CFD. Both methods showed the aerodynamic phenomenon with their own unique visualization. The experimental method used the wool tuft to visualize whether and where the separation between airflow and the surface of the body occurred, which was create wakes and therefore created drag force. Wool tuft will vibrate to indicate where the separation occurred. This vibration of the wool tuft began at the middle of the models and continue along the body until at the rear end of the models. CFD method used colors to visualize the pressure difference in all sections required. Pressure difference could lead to a stagnation point and separation point. Stagnation point occurred on the front section of the models and separation point occurred between the middle section of the models until the rear end of the models.

Designing the shape of a car body was crucial in order to reduce the  $C_D$  value, especially for low-energy prototype class cars, which was the object of this study. Begin with the front section of the car, the best shape achieved at this study in order to reduce drag was the lower nose shape. At the rear, the best shape was a smaller tail form. Both shapes were applied to JM-4 and successfully contributed 7.64% in drag reduction compared to the initial design. The front and rear wheel of the car also contributes to the creation of drag so it should be covered. The covered front wheel contributed 13.67% from the uncovered front wheel, while the covered rear wheel contributed 26.73% from the uncovered rear wheel in an attempt to reduce drag. Overall, this study obtained the lowest  $C_D$  value of 0.202 on the final design (JM-4 v2).

## **Acknowledgment**

The authors would like to acknowledge the help and support of the National Laboratory for Aerodynamics, Aeroelastics, and Aeroacoustics Technology, Research Center for Science and Technology.

## References

- [1] KMHE committee, Tentang KMHE. [Online]. Available: <http://kmhe2017.its.ac.id/info>. [Accessed: Oct. 14, 2017].
- [2] J. J. Santin, C. H. Onder, J. Bernard, D. Isler, P. Kobler, F. Kolb, N. Weidmann, L. Guzzella, *The World's Most Fuel Efficient Vehicle: Design and Development of PAC CAR II*, 1st ed. Zurich: vdfHochschulverlag, 2007. [Online].
- [3] F. Eugene, *Development of An Aerodynamic Carbon Fiber Vehicle Body for Shell Eco-Marathon 2012 Prototype Category*, Mapua: Mapua Institute of Technology, 2012.
- [4] W. Danek, "Determination of The Drag Coefficient High Performance Electric Vehicle," *Modelowanie Inzynierskie* (1), 36-41 (2013).
- [5] E. Abo-Serie and E. Oran, "Aerodynamic Considerations for A Low Drag Shell Eco-Marathon Competition Car," *International Conference on Automation and Mechatronics Engineering (ICAME)* 2016.
- [6] A. Cieśliński, W. Prym, M. Stajuda, D. Witkowski, "Investigation on Aerodynamics of Super-Effective Car for Drag Reduction," *Mechanics and Mechanical Engineering* (20), 295-308 (2012).
- [7] T. S. Utomo and J. S. Jhon S., "Analisis Aerodinamika Body Mobil Hemat Energi Antawirya Residual-Sat Dengan Menggunakan Metode Computational Fluid Dynamics," *Jurnal Teknik Mesin S-1*(5), 50-59 (2017).
- [8] J. D. Anderson, *Fundamentals of Aerodynamics*, 2nd ed. New York: McGraw-Hill Inc., 1991.
- [9] J. Katz, *Race Car Aerodynamics: Designing for Speed*, 2nd ed. Massachusetts: Bentley Publisher, 1995.
- [10] Gillespie, D. Thomas, *Fundamentals of Vehicle Dynamics*, 4th ed. Denvers: Society of Automotive Engineers, Inc., 1992.